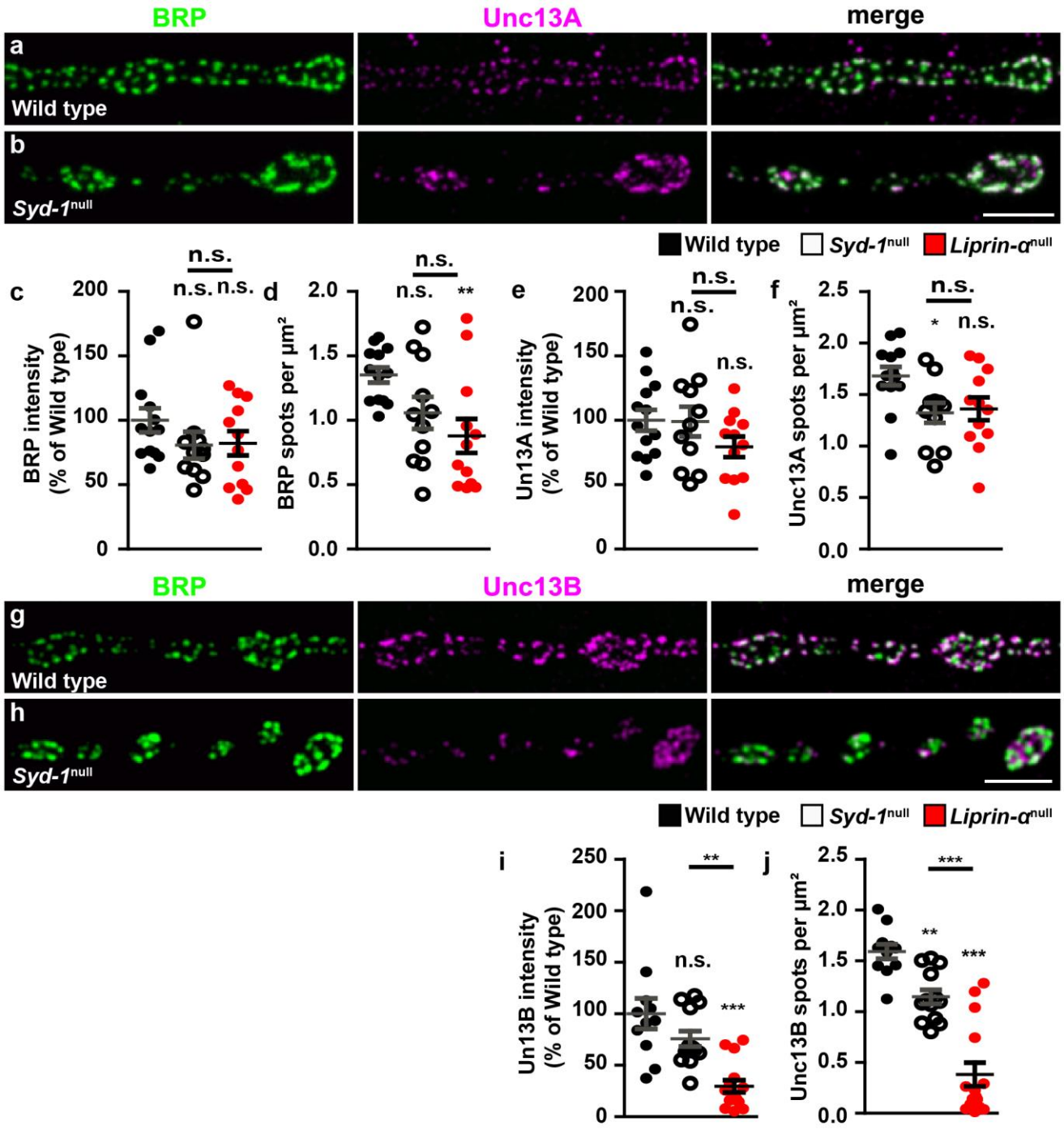

Supplementary Figure 1

Liprin-α/Syd-1 scaffold complexes organize the AZ localization of Unc13B

(**a,b**) Muscle 4 NMJs of segments A2-A4 from 3rd instar larvae of the displayed genotypes labelled with the antibodies (ABs) indicated. (**c**) Mean BRP intensity measured over the whole NMJ was unchanged in *Syd-1*^{null} and *Liprin-α*^{null} in comparison to the Wild type (Wild type (n=13 NMJs from 4 larvae) vs. *Syd-1*^{null} (n=11 NMJs from 4 larvae) vs. *Liprin-α*^{null} (n=12 NMJs from 4 larvae): p >0.05 for Wild type vs *Syd-1*^{null}; p >0.05 for Wild type vs. *Liprin-α*^{null}; p >0.05 for *Syd-1*^{null} vs. *Liprin-α*^{null}; p=0.2883 (F(2,33)=1.29)). (**d**) BRP spots per µm² NMJ were slightly reduced in *Syd-1*^{null} and significantly reduced in *Liprin-α*^{null} in comparison to the Wild type (Wild type (n=13 NMJs from 4 larvae) vs. *Syd-1*^{null} (n=11 NMJs from 4 larvae) vs. *Liprin-α*^{null} (n=12 NMJs from 4 larvae): p >0.05 for Wild type vs *Syd-1*^{null}; p ≤0.01 for Wild type vs. *Liprin-α*^{null}; p >0.05 for *Syd-1*^{null} vs. *Liprin-α*^{null}; p=0.0108 (F(2,33)=5.207)). (**e**) Mean Unc13A intensity measured

over the whole NMJ was unchanged in *Syd-1*^{null} and *Liprin-α*^{null} in comparison to the Wild type (Wild type (n=13 NMJs from 4 larvae) vs. *Syd-1*^{null} (n=11 NMJs from 4 larvae) vs. *Liprin-α*^{null} (n=12 NMJs from 4 larvae): p >0.05 for Wild type vs *Syd-1*^{null}; p >0.05 for Wild type vs. *Liprin-α*^{null}; p >0.05 for *Syd-1*^{null} vs. *Liprin-α*^{null}; p=0.2105 (F(2,33)=1.63)). (**f**) Unc13A spots per µm² NMJ were slightly reduced in *Syd-1*^{null} and *Liprin-α*^{null} in comparison to the Wild type (Wild type (n=13 NMJs from 4 larvae) vs. *Syd-1*^{null} (n=11 NMJs from 4 larvae) vs. *Liprin-α*^{null} (n=12 NMJs from 4 larvae): p ≤0.05 for Wild type vs *Syd-1*^{null}; p >0.05 for Wild type vs. *Liprin-α*^{null}; p >0.05 for *Syd-1*^{null} vs. *Liprin-α*^{null}; p=0.0278 (F(2,33)=4.00)). (**g,h**) Muscle 4 NMJs of segments A2-A4 from 3rd instar larvae of the displayed genotypes labelled with the ABs indicated. (**i**) Mean Unc13B intensity measured over the whole NMJ was slightly reduced in *Syd-1*^{null} but severely reduced in *Liprin-α*^{null} in comparison to the Wild type (Wild type (n=13 NMJs from 5 larvae) vs. *Syd-1*^{null} (n=11 NMJs from 5 larvae) vs. *Liprin-α*^{null} (n=15 NMJs from 5 larvae): p >0.05 for Wild type vs *Syd-1*^{null}; p ≤0.001 for Wild type vs. *Liprin-α*^{null}; p ≤0.01 for *Syd-1*^{null} vs. *Liprin-α*^{null}; p <0.0001 (F(2,36)=15.13)). (**j**) Unc13B spots per µm² NMJ were significantly reduced in *Syd-1*^{null} but severely reduced in *Liprin-α*^{null} in comparison to the Wild type (Wild type (n=13 NMJs from 5 larvae) vs. *Syd-1*^{null} (n=11 NMJs from 5 larvae) vs. *Liprin-α*^{null} (n=15 NMJs from 5 larvae): p ≤0.01 for Wild type vs *Syd-1*^{null}; p ≤0.001 for Wild type vs. *Liprin-α*^{null}; p ≤0.001 for *Syd-1*^{null} vs. *Liprin-α*^{null}; p <0.0001 (F(2,36)=42.93)). Number and p values are listed in Supplementary Table 1. Statistics for c-f, i, j: nonparametric one-way analysis of variance (ANOVA) test, followed by a Turkey's multiple comparison test. All panels show mean ± SEM; *, p ≤0.05; **, p ≤0.01; ***, p ≤0.001; ns, not significant, p >0.05. Scale bars: 5 µm.

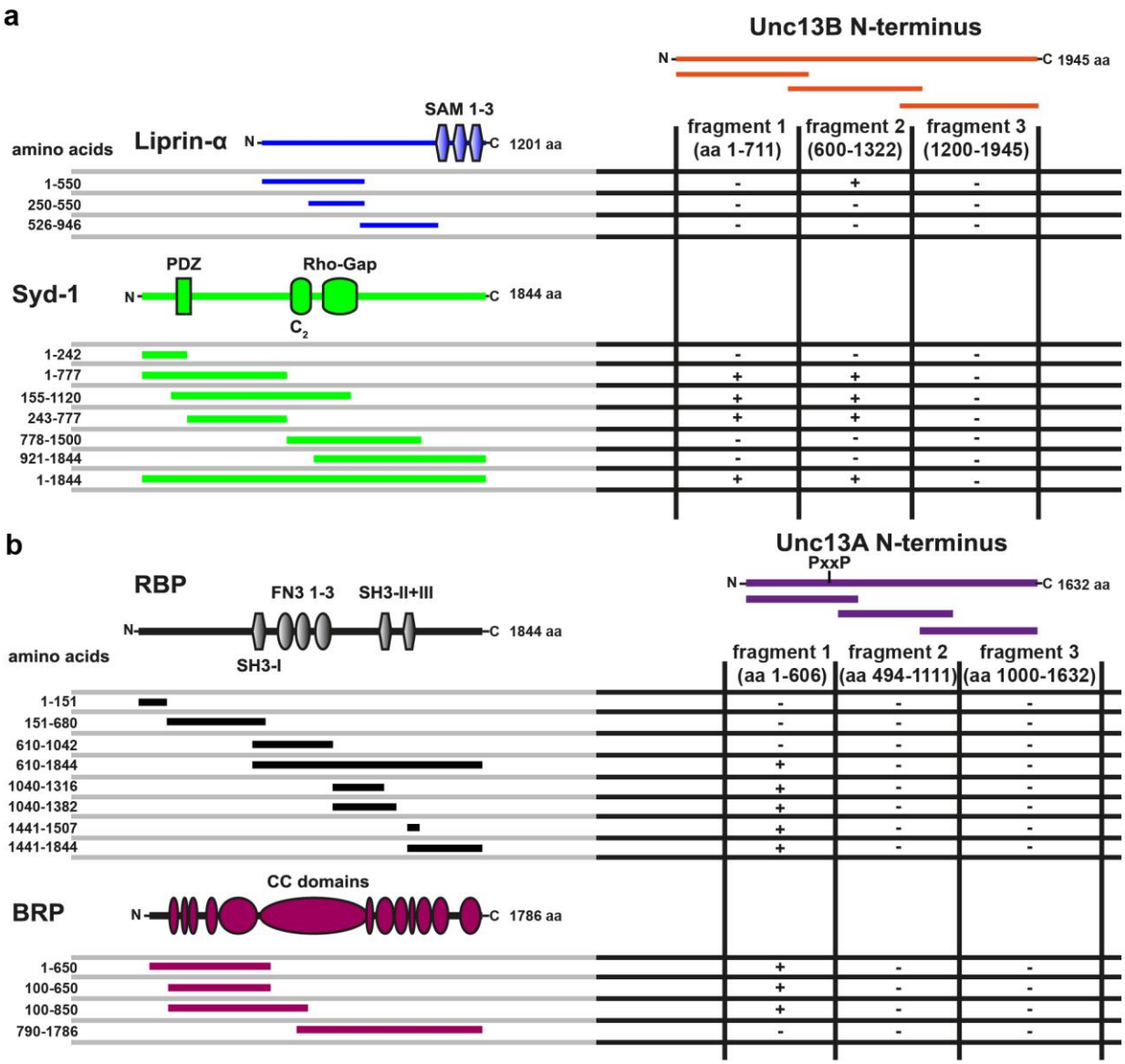

Supplementary Figure 2

Unc13B interacts with Syd-1/Liprin-α; Unc13A interacts with BRP/RBP

(**a**) Schematic representation of Unc13B N-terminus including three fragments (1-3) that were used in the Y2H screen; Liprin-α domain structure containing three C-terminal SAM domains (I-III from the N terminus); Syd-1 domain structure containing an N-terminal PDZ domain, a C_2 and a Rho-GAP domain. The corresponding fragments of each protein used in the Y2H screen are indicated. A central N-terminal fragment of Unc13B interacted with an N-terminal part of Liprin-α. Both very N-terminal fragments of Unc13B interacted with a central stretch of Syd-1 located in-between PDZ- and C_2-domain. (**b**) Schematic representation of Unc13A N-terminus including three fragments (1-3) that were used in the Y2H screen. The RBP-binding PxxP motif is indicated; RBP domain structure containing three SH3 domains (I-III from the N terminus) and three Fibronectin 3 (FN3) domains; BRP domain structure containing several coiled-coil (CC) domains. The corresponding fragments of each protein used in the Y2H screen are indicated. The most N-terminal fragment of Unc13A (including the RBP binding PxxP motif) interacted with both C-terminal fragments of RBP including the SH3-domains II and III, and with an N-terminal part of BRP.

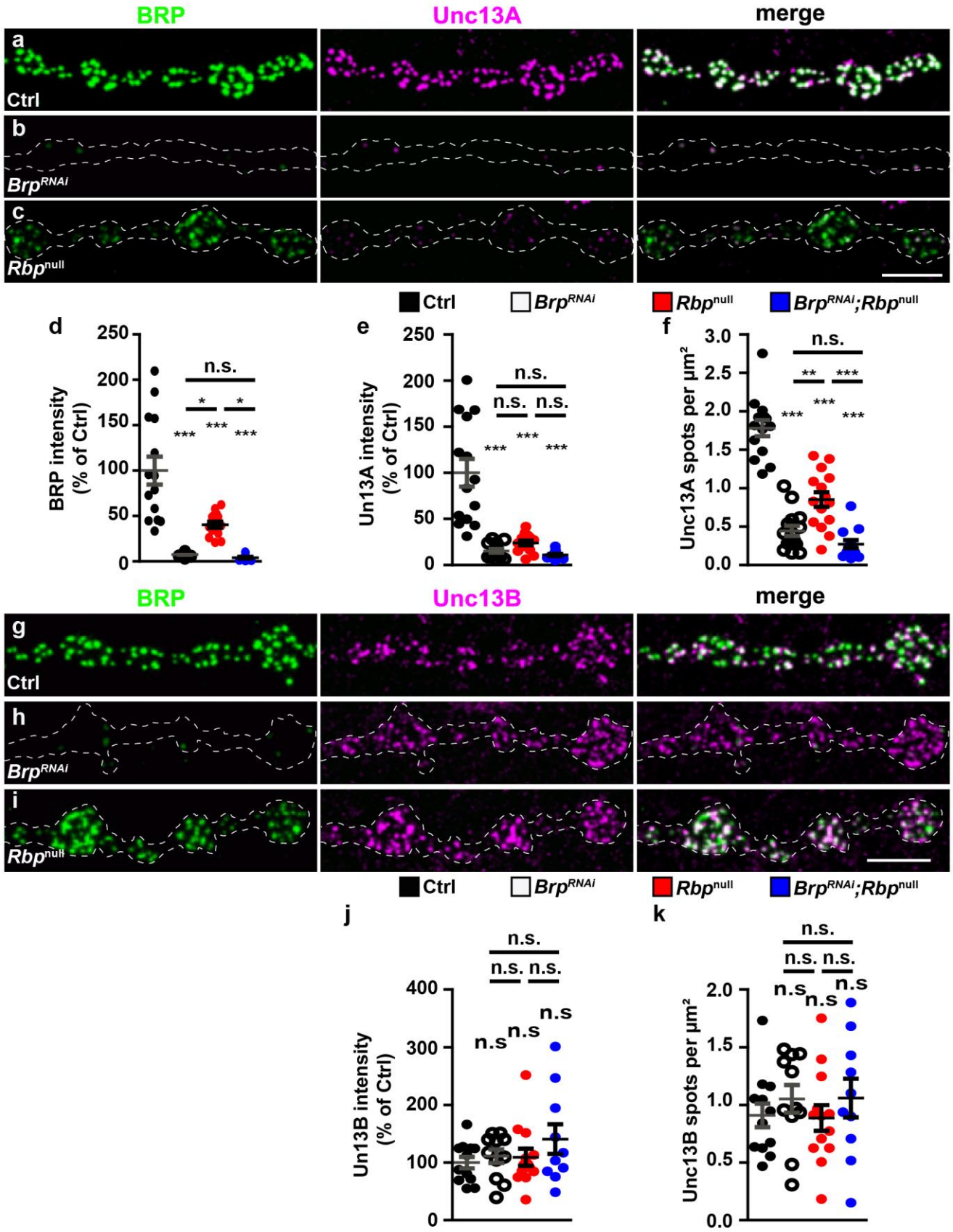

Nature Neuroscience: doi:10.1038/nn.4364

Supplementary Figure 3

BRP/RBP scaffold complexes organize the AZ-localization of Unc13A

(**a-c**) Muscle 4 NMJs of segments A2-A4 from 3rd instar larvae of the displayed genotypes labelled with the ABs indicated. BRP as well as Unc13A were severely decreased upon motoneuronal downregulation of BRP or in Rbp^{null} mutants. (**d,e**) BRP as well as Unc13A intensity were severely decreased upon motoneuronal downregulation of BRP or in Rbp^{null} mutants with the strongest downregulation upon *Brp* knockdown in Rbp^{null} (BRP intensity: Ctrl (n=14 NMJs from 5 larvae) vs. Brp^{RNAi} (n=15 NMJs from 5 larvae) vs. Rbp^{null} (n=15 NMJs from 5 larvae) vs. $Brp^{RNAi};RBP^{null}$ (n=13 NMJs from 5 larvae): p ≤0.001 for Ctrl vs Brp^{RNAi}; p ≤0.001 for Ctrl vs. Rbp^{null}; p ≤0.001 for Ctrl vs. $Brp^{RNAi};RBP^{null}$; p ≤0.05 for Brp^{RNAi} vs. Rbp^{null}; p >0.05 for Brp^{RNAi} vs. $Brp^{RNAi};RBP^{null}$; p ≤0.05 for Rbp^{null} vs. $Brp^{RNAi};RBP^{null}$; p <0.0001 (F(3,53)=31.96)); Unc13A intensity: Ctrl (n=14 NMJs from 5 larvae) vs. Brp^{RNAi} (n=15 NMJs from 5 larvae) vs. Rbp^{null} (n=15 NMJs from 5 larvae) vs. $Brp^{RNAi};RBP^{null}$ (n=13 NMJs from 5 larvae): p ≤0.001 for Ctrl vs Brp^{RNAi}; p ≤0.001 for Ctrl vs. Rbp^{null}; p ≤0.001 for Ctrl vs. $Brp^{RNAi};RBP^{null}$; p >0.05 for Brp^{RNAi} vs. Rbp^{null}; p >0.05 for Brp^{RNAi} vs. $Brp^{RNAi};RBP^{null}$; p >0.05 for Rbp^{null} vs. $Brp^{RNAi};RBP^{null}$; p <0.0001 (F(3,53)=30.07)). (**f**) Unc13A spots per µm² NMJ were decreased upon motoneuronal downregulation of BRP or in Rbp^{null} mutants with the strongest downregulation upon *Brp* knockdown in Rbp^{null} (Ctrl (n=14 NMJs from 5 larvae) vs. Brp^{RNAi} (n=15 NMJs from 5 larvae) vs. Rbp^{null} (n=15 NMJs from 5 larvae) vs. $Brp^{RNAi};RBP^{null}$ (n=13 NMJs from 5 larvae): p ≤0.001 for Ctrl vs Brp^{RNAi}; p ≤0.001 for Ctrl vs. Rbp^{null}; p ≤0.001 for Ctrl vs. $Brp^{RNAi};RBP^{null}$; p ≤0.01 for Brp^{RNAi} vs. Rbp^{null}; p >0.05 for Brp^{RNAi} vs. $Brp^{RNAi};RBP^{null}$; p ≤0.001 for Rbp^{null} vs. $Brp^{RNAi};RBP^{null}$; p <0.0001 (F(3,53)=63.28)). (**g-i**) Muscle 4 NMJs of segments A2-A4 from 3rd instar larvae of the genotypes indicated labelled with the ABs indicated. BRP but not Unc13B were severely decreased upon motoneuronal downregulation of BRP as well as in Rbp^{null} mutants. (**j**) Mean Unc13B intensity measured over the whole NMJ was not affected upon downregulation of BRP or in Rbp^{null} mutants or even upon *Brp* knockdown in Rbp^{null} (Ctrl (n=12 NMJs from 5 larvae) vs. Brp^{RNAi} (n=11 NMJs from 5 larvae) vs. Rbp^{null} (n=13 NMJs from 5 larvae) vs. $Brp^{RNAi};RBP^{null}$ (n=10 NMJs from 5 larvae): p >0.05 for Ctrl vs Brp^{RNAi}; p >0.05 for Ctrl vs. Rbp^{null}; p >0.05 for Ctrl vs. $Brp^{RNAi};RBP^{null}$; p >0.05 for Brp^{RNAi} vs. Rbp^{null}; p >0.05 for Brp^{RNAi} vs. $Brp^{RNAi};RBP^{null}$; p >0.05 for Rbp^{null} vs. $Brp^{RNAi};RBP^{null}$; p=0.3491 (F(3,42)=1.127)). (**k**) Unc13B spots per µm² NMJ were unchanged upon downregulation of BRP or in Rbp^{null} mutants or even upon *Brp* knockdown in Rbp^{null} (Ctrl (n=12 NMJs from 5 larvae) vs. Brp^{RNAi} (n=11 NMJs from 5 larvae) vs. Rbp^{null} (n=13 NMJs from 5 larvae) vs. $Brp^{RNAi};RBP^{null}$ (n=10 NMJs from 5 larvae): p >0.05 for Ctrl vs Brp^{RNAi}; p >0.05 for Ctrl vs. Rbp^{null}; p >0.05 for Ctrl vs. $Brp^{RNAi};RBP^{null}$; p >0.05 for Brp^{RNAi} vs. Rbp^{null}; p >0.05 for Brp^{RNAi} vs. $Brp^{RNAi};RBP^{null}$; p >0.05 for Rbp^{null} vs. $Brp^{RNAi};RBP^{null}$; p=0.6570 (F(3,42)=0.5408)). Number and p values are listed in Supplementary Table 1. Statistics for d-f, j,k: nonparametric one-way analysis of variance (ANOVA) test, followed by a Turkey's multiple comparison test. All panels show mean ± SEM; *, p ≤0.05; **, p ≤0.01; ***, p ≤0.001; ns, not significant, p >0.05. Scale bars: 5 µm.

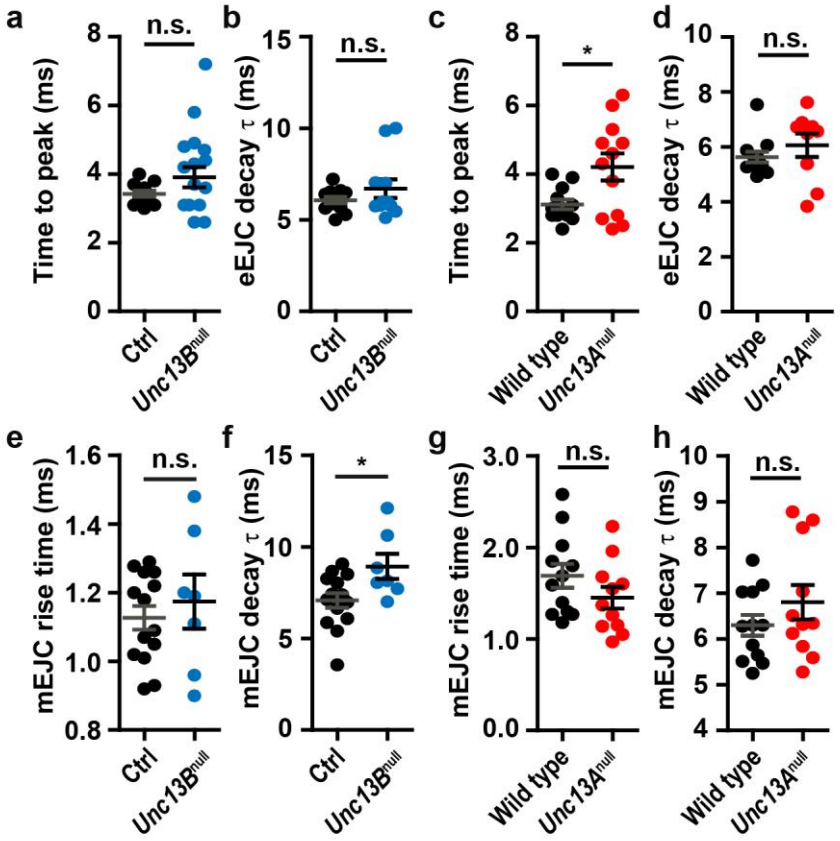

Supplementary Figure 4

TEVC analysis of Unc13A and Unc13B mutant terminals

(**a,b**) The time-to-peak (time difference between stimulation pulse to the afferent nerve and the eEJC minimum) and eEJC decay, which is the time constant τ resulting from a single exponential fit in the range from 60% of the eEJC amplitude back to baseline, both are similar in Ctrl (black) and *Unc13B*^{null} (blue) (time to peak: Ctrl (n=12 NMJs from 12 larvae) vs *Unc13B*^{null} (n=12 NMJs from 12 larvae), p=0.1333 (t(22)=1.559); eEJC decay: Ctrl (n=12 NMJs from 12 larvae) vs *Unc13B*^{null} (n=11 NMJs from 11 larvae), p=0.2413 (t(21)=1.206)). (**c**) The time to peak is significantly prolonged in *Unc13A*^{null} mutant synapses (Wild type (n=12 NMJs from 12 larvae) vs *Unc13A*^{null} (n=12 NMJs from 12 larvae), p=0.0162 (t(22)=2.605)). (**d**) The eEJC decay is similar in Wild type and *Unc13A*^{null} (Wild type (n=12 NMJs from 12 larvae) vs *Unc13A*^{null} (n=9 NMJs from 9 larvae), p=0.2136 (U=36)). (**e**) The mEJC rise time is unaltered in *Unc13B*^{null} mutant synapses compared to Ctrl (Ctrl (n=14 NMJs from 10 larvae) vs *Unc13B*^{null} (n=7 NMJs from 5 larvae), p=0.7652 (U=44.5)). (**f**) In *Unc13B*^{null} the mEJC decay is significantly increased compared to Ctrl (Ctrl (n=14 NMJs from 10 larvae) vs *Unc13B*^{null} (n=7 NMJs from 5 larvae), p=0.0480 (U=22.00)). (**g,h**) mEJC kinetics do not differ between Wild type and *Unc13A*^{null} (mEJC rise time: Wild type (n=12 NMJs from 6 larvae) vs *Unc13A*^{null} (n=11 NMJs from 6 larvae), p=0.1914 (t(21)=1.350); mEJC decay: Wild type (n=12 NMJs from 6 larvae) vs *Unc13A*^{null} (n=11 NMJs from 6 larvae), p=0.2546 (t(21)=1.171)). All recordings were performed in the presence of 1.5 mM extracellular Ca^{2+}. Number and p values are listed in Supplementary Table 1. Statistics: Student's t-test besides panels d,e,f where a Mann Whitney U-test was performed. All panels show mean ± SEM; *, p ≤0.05; **, p ≤0.01; ***, p ≤0.001; ns, not significant, p >0.05.

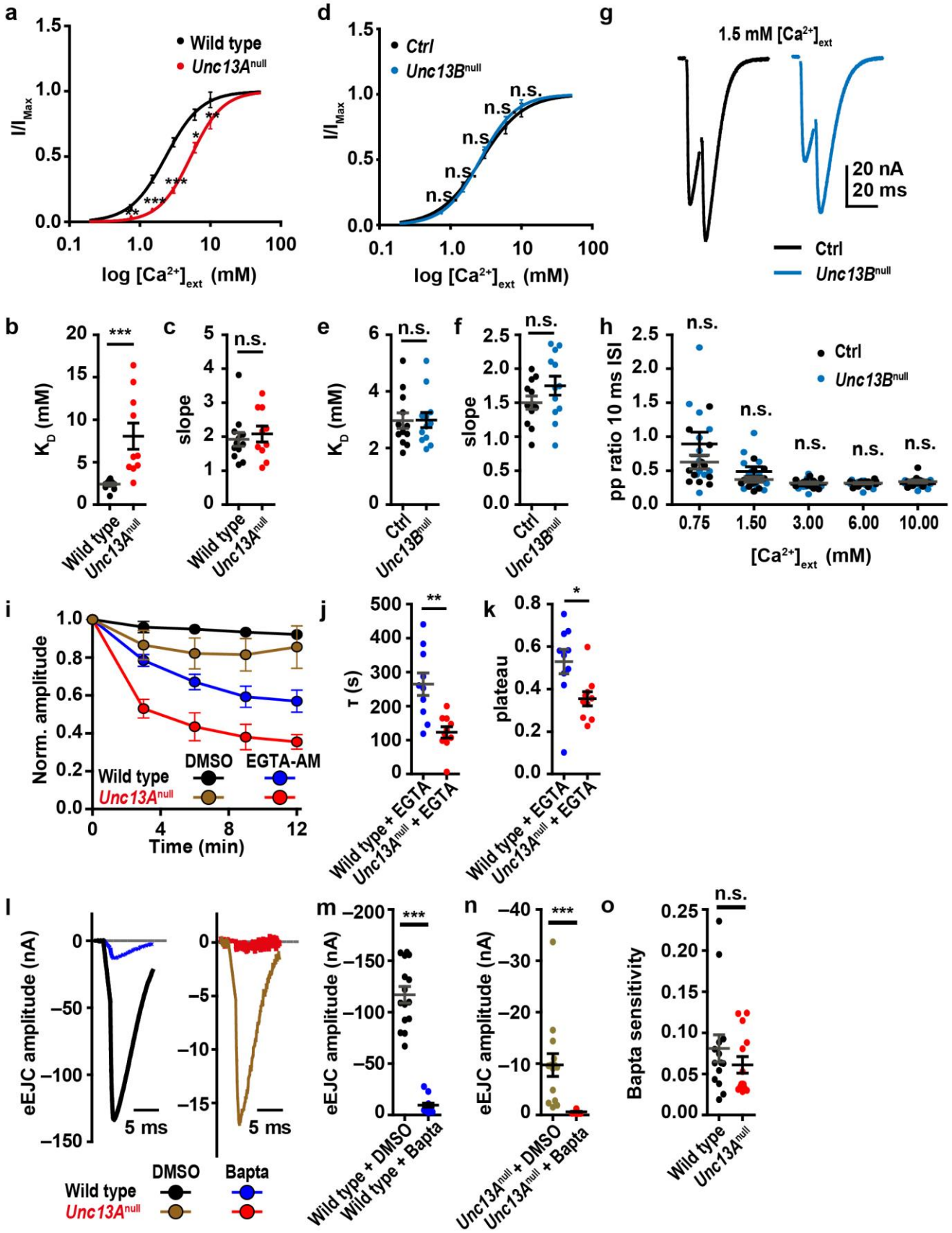

Nature Neuroscience: doi:10.1038/nn.4364

Supplementary Figure 5

Ca^{2+} sensitivity and release probability is altered upon loss of Unc13A but not -B

(**a-f**) Plot of eEJC amplitude as a function of extracellular Ca^{2+} concentrations $[Ca^{2+}]_{ext}$ fitted with Hill equations to determine the values for slope and K_D. A clear shift can be observed in (a) *Unc13A*^{null} mutant synapses (red) compared to Wild type (black), whereas in (d) there is no change upon loss of *Unc13B*^{null} (blue) compared to Ctrl (black) (a: Wild type (n=12 NMJs from 12 larvae per Ca^{2+} concentration) vs *Unc13A*^{null} (n=10 NMJs from 10 larvae per Ca^{2+} concentration): 0.75 mM $[Ca^{2+}]_{ext}$: p=0.0092 (U=20); 1.5 mM $[Ca^{2+}]_{ext}$: p <0.0001 (U=0); 3 mM $[Ca^{2+}]_{ext}$: p=0.0005 (U=7); 6 mM $[Ca^{2+}]_{ext}$: p=0.0272 (U=26); 10 mM $[Ca^{2+}]_{ext}$: p=0.0062 (U=18)); d: Ctrl (n=12 NMJs from 12 larvae per Ca^{2+} concentration) vs *Unc13B*^{null} (n=12 NMJs from 12 larvae per Ca^{2+} concentration): 0.75 mM $[Ca^{2+}]_{ext}$: p=0.1971 (t(22)=1.330); 1.5 mM $[Ca^{2+}]_{ext}$: p=0.2652 (t(22)=1.143); 3 mM $[Ca^{2+}]_{ext}$: p=0.9269 (t(22)=0.09278); 6 mM $[Ca^{2+}]_{ext}$: p=0.5181 (t(22)=0.6569); 10 mM $[Ca^{2+}]_{ext}$: p=0.6284 (t(22)=0.4908)). The values for I/I_{max} can be found in Supplementary Table 1. (**b**) Ca^{2+}-dependence of release analysis revealed an increased Ca^{2+} requirement (K_D, obtained from fitting with the Hill function) in *Unc13A*^{null} mutant synapses (Wild type (n=12 NMJs from 12 larvae) vs *Unc13A*^{null} (n=10 NMJs from 10 larvae), p=0.0004 (U=6)). (**c**) The apparent Ca^{2+} cooperativity of release (slope, obtained from fitting with the Hill function) is not different in *Unc13A*^{null} relative to Wild type (Wild type (n=12 NMJs from 12 larvae) vs *Unc13A*^{null} (n=10 NMJs from 10 larvae), p=0.6682 (U=53)). (**e,f**) The Ca^{2+}-dependence and Ca^{2+}-cooperativity of release are both unaltered upon loss of Unc13B (K_D: Ctrl (n=12 NMJs from 12 larvae) vs *Unc13B*^{null} (n=12 NMJs from 12 larvae), p=0.9566 (t(22)=0.05502); slope: Ctrl (n=12 NMJs from 12 larvae) vs *Unc13B*^{null} (n=12 NMJs from 12 larvae), p=0.1574 (t(22)=1.464)). (**g**) Sample traces of paired pulse stimulation for Ctrl (black) and *Unc13B*^{null} (blue) at 10 ms ISI show no differences between genotypes. (**h**) The paired pulse ratios were not significantly changed in *Unc13B*^{null} at 10 ms ISI, in all Ca^{2+} concentrations (Ctrl (n=12 NMJs from 12 larvae per Ca^{2+} concentration) vs *Unc13B*^{null} (n=12 NMJs from 12 larvae per Ca^{2+} concentration): 0.75 mM $[Ca^{2+}]_{ext}$: p=0.1971 (t(22)=1.33); 1.5 mM $[Ca^{2+}]_{ext}$: p=0.1678 (t(22)=1.426); 3 mM $[Ca^{2+}]_{ext}$: p=0.474 (t(22)=0.7284); 6 mM $[Ca^{2+}]_{ext}$: p=0.3726 (t(22)=0.9102); 10 mM $[Ca^{2+}]_{ext}$: p=0.2602 (t(22)=1.156)). Values can be found in Supplementary Table 1. (**i**) *Unc13A*^{null} (gold: control with DMSO, red: with EGTA-AM/DMSO) shows faster and stronger inhibition of eEJC amplitudes after addition of 200 µM EGTA-AM to the extra-cellular solution compared to Wild type (black: control with DMSO, blue: with EGTA-AM/DMSO). Amplitudes are normalized to average eEJC amplitudes obtained during 1 min of baseline recording prior to the addition of EGTA-AM/DMSO or DMSO, each with Pluronic F-127. Synaptic transmission was stimulated by single action potentials every 10 s. Experiments were performed in the presence of 2.5 mM extracellular Ca^{2+}. Values can be found in Supplementary Table 1. (**j**) The time constant of the inhibition caused by EGTA-AM application was determined by fitting a single exponential decay function to 100 peak amplitude values after addition of EGTA-AM in individual cells. This revealed a significantly faster inhibition in *Unc13A*^{null} compared to Wild type animals (Wild type + EGTA (n=10 NMJs from 10 larvae) vs *Unc13A*^{null} + EGTA (n=10 NMJs from 10 larvae), p=0.0012 (t(18)=3.835)). (**k**) The asymptotic inhibition is captured in the exponential fit as the plateau value which was significantly decreased in *Unc13A*^{null} in comparison to Wild type (Wild type + EGTA (n=10 NMJs from 10 larvae) vs *Unc13A*^{null} + EGTA (n=10 NMJs from 10 larvae), p=0.016 (t(18)=2.6508)). (**l**) 30 min incubation with the fast Ca^{2+}-buffer Bapta-AM reduced eEJC amplitudes in both genotypes to a similar extent. Sample traces for Wild type (black with DMSO, blue with Bapta-AM/DMSO) and *Unc13A*^{null} (gold with DMSO, red with Bapta-AM/DMSO) exhibit similar Bapta-sensitivity for both genotypes. For clarity, the stimulation artefact was removed and replaced by a straight line. (**m,n**) The significant reduction of the eEJC amplitude after 30 min Bapta-AM incubation is similar in Wild type (m) and *Unc13A*^{null} (n) compared to DMSO incubated cells (m: Wild type + DMSO (n=15 NMJs from 9 larvae) vs Wild type + Bapta (n=14 NMJs from 9 larvae), p <0.0001 (t(27)=12.59); n: *Unc13A*^{null} + DMSO (n=14 NMJs from 10 larvae) vs *Unc13A*^{null} + Bapta (n=14 NMJs from 8 larvae), p=0.0004 (t(26)=4.095)). Values can be found in Supplementary Table 1. (**o**) The Bapta sensitivity is calculated as the ratio of eEJC amplitude size in the presence of Bapta-AM/DMSO to the eEJC amplitude size in the presence of DMSO. The Bapta-sensitivity does not differ between Wild type and *Unc13A*^{null} (Bapta sensitivity: Wild type (n=14 NMJs from 9 larvae) vs *Unc13A*^{null} (n=14 NMJs from 8 larvae), p=0.304 (t(26)=1.049)). Values can be found in Supplementary Table 1. Statistics: Student's t-test except for panels (a-c) where a Mann-Whitney U-test was performed. All panels show mean ± SEM; *, p ≤0.05; **, p ≤0.01; ***, p ≤0.001; ns, not significant, p >0.05.

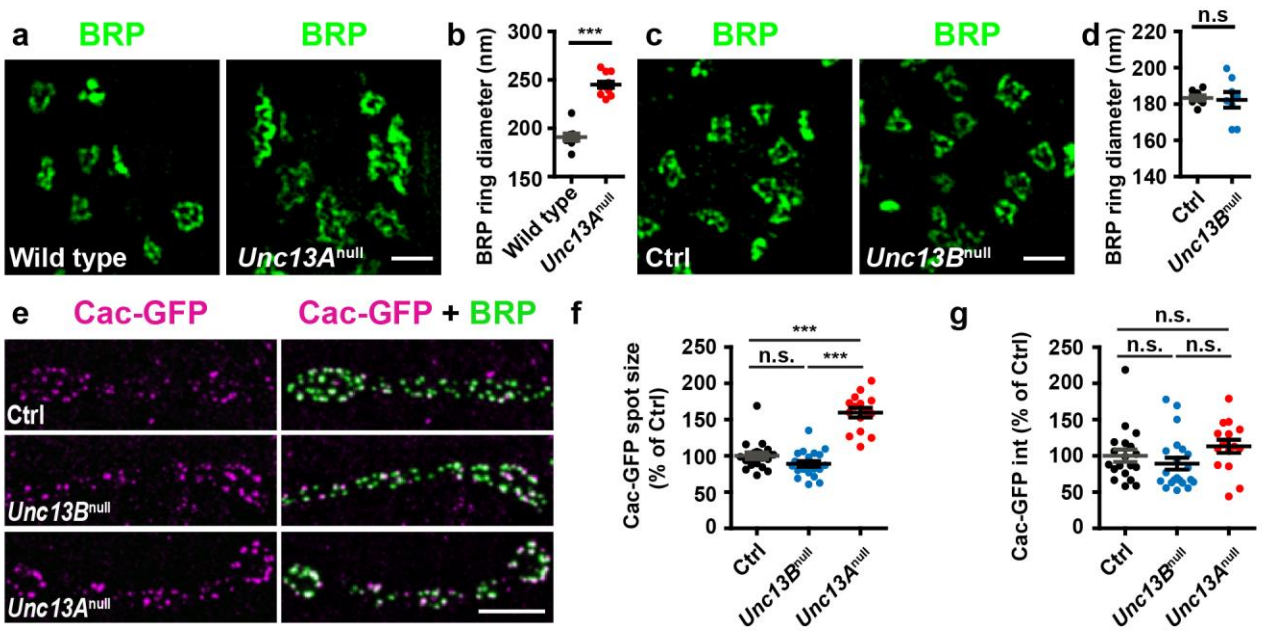

Supplementary Figure 6

Increased Ca^{2+} channel abundance at *Unc13A*^{null} mutant AZs

(**a**) Two-color STED images of multiple AZs from 3rd instar larvae of the displayed genotypes labelled with the indicated ABs. BRP rings were larger in *Unc13A*^{null}. (**b**) BRP ring diameters were increased in *Unc13A*^{null} in comparison to the Wild type (Wild type (n=9 NMJs from 3 larvae) vs *Unc13A*^{null} (n=12 NMJs from 3 larvae), p=0.0001 (U=0)). (**c**) Two-color STED images of multiple AZs from 3rd instar larvae of the displayed genotypes labelled with the indicated ABs. BRP ring structure appeared normal in *Unc13B*^{null} (**d**) BRP ring diameters were unchanged in *Unc13B*^{null} in comparison to Ctrl (Ctrl (n=8 NMJs from 3 larvae) vs *Unc13B*^{null} (n=8 NMJs from 3 larvae), p=0.9591 (U=31)). (**e**) Muscle 4 NMJs of segments A2-A4 from 3rd instar larvae of the displayed genotypes labelled with the ABs indicated. (**f**) Cac-GFP spot sizes were increased in *Unc13A*^{null} but not *Unc13B*^{null} in comparison to Ctrl (Ctrl (n=19 NMJs from 5 larvae) vs. *Unc13A*^{null} (n=15 NMJs from 5 larvae) vs. *Unc13B*^{null} (n=21 NMJs from 5 larvae): p >0.05 for Ctrl vs *Unc13B*^{null}; p ≤0.001 for Ctrl vs. Unc13A^{null}; p ≤0.001 for *Unc13B*^{null} vs. *Unc13A*^{null}; p <0.0001 (F(2,52)=54.12)). (**g**) Mean Cac-GFP intensity measured over the whole NMJ was similar in *Unc13A*^{null}, *Unc13B*^{null} and Ctrl (Ctrl (n=19 NMJs from 5 larvae) vs. *Unc13A*^{null} (n=15 NMJs from 5 larvae) vs. *Unc13B*^{null} (n=21 NMJs from 5 larvae): p >0.05 for Ctrl vs *Unc13B*^{null}; p >0.05 for Ctrl vs. Unc13A^{null}; p >0.05 for *Unc13B*^{null} vs. *Unc13A*^{null}; p=0.166 (F(2,52)=1.855)). Number and p values are listed in Supplementary Table 1. Statistics: Mann-Whitney U-test, except for f and g where a nonparametric one-way analysis of variance (ANOVA) test, followed by a Turkey's multiple comparison test was performed. All panels show mean ± SEM; *, p ≤0.05; **, p ≤0.01; ***, p ≤0.001; ns, not significant, p >0.05. Scale bar: (a,c) 500 nm; (e) 5 µm.

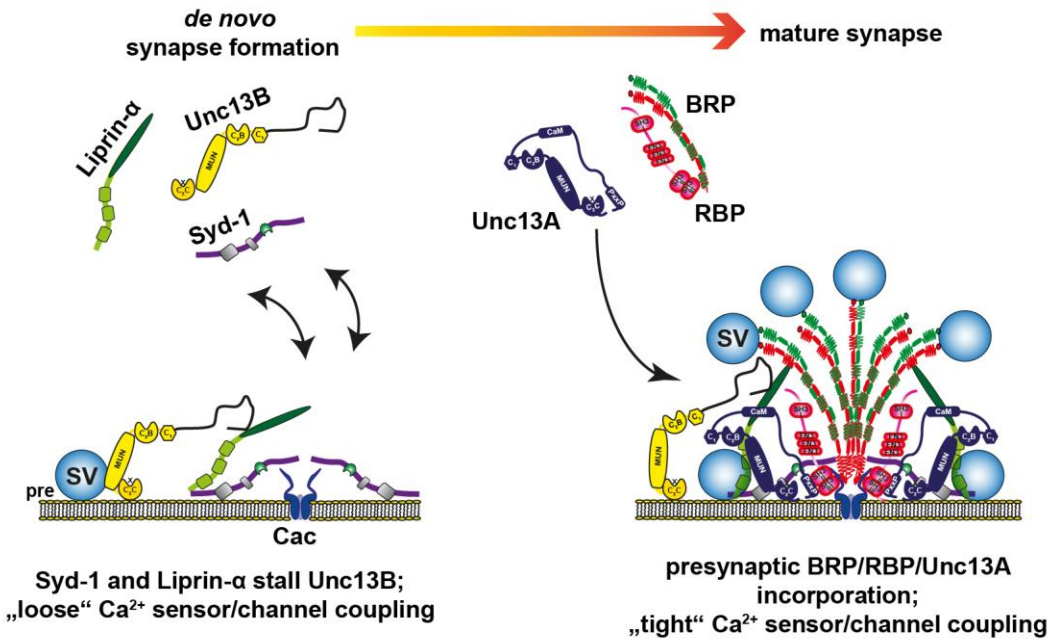

Supplementary Figure 7

Sketch of *de novo* synapse formation

During the process of AZ assembly, clusters of Syd-1 and Liprin-α undergo rounds of assembly and disassembly at the presynaptic membrane. Unc13B localizes to sites of *de novo* synapse formation via the Syd-1/Liprin-α scaffold. At nascent synapses, this induces a loose SV-Ca^{2+} channel coupling. Later during the AZ maturation process, Unc13A localizes to more mature synapses via a second, central RBP/BRP scaffold that concentrates Unc13A at the center of the AZ. Unc13A facilitates a close localization of SVs to the presynaptic Ca^{2+} channels and therefore maintains a tight stimulus/secretion coupling.

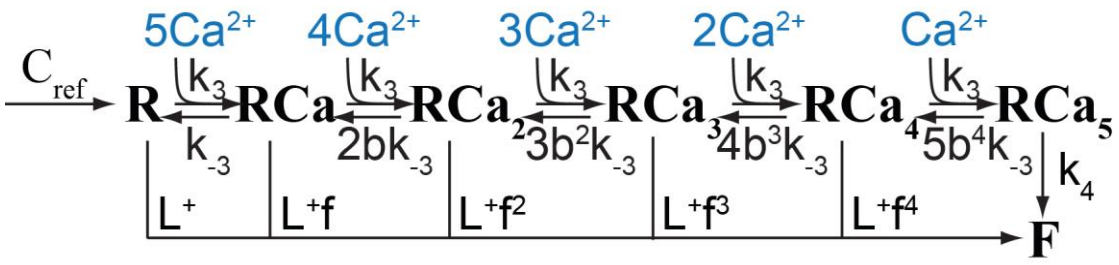

Supplementary Figure 8

Allosteric five-site binding model of Ca^{2+}-driven exocytosis

Reaction scheme (derived from the 'allosteric model'; Lou et al., 2005. Nature. 435:497-501) depicts the sequential binding of up to five Ca^{2+} ions to a single vesicle (RCa_{0-5}).

Supplementary Table 1

Summary of all obtained parameters in this study

Light microscopy: CLSM (Fig. 1, 3; Fig. S1, S2, S5)		**mean ± SEM**			
Parameter (Figure)	**Description**	**control (n)**	**mutant (n)**	**P**	**(test)**
AZ density (Fig. 1)	BRP spots/µm^2				
Unc13A^{null} (Fig.1o)		1.658 ± 0.079 (19)	1.207 ± 0.063 (23)	≤0.001***	(Mann-Whitney U-test)
Unc13B^{null} (Fig.1p)		1.559 ± 0.070 (28)	1.354 ± 0.055 (35)	≤0.05*	(Mann-Whitney U-test)
mean BRP intensity (Fig. S1c; S3d)	measured over the whole NMJ (% of Wild type)				
in *Syd-1*^{null} (Fig. S1c)		100.0 ± 9.269 (13)	80.62 ± 10.390 (11)	n.s.	(ANOVA test, followed by a Turkey's multiple comparison test)
in *Liprin-α*^{null} (Fig. S1c)			82.13 ± 9.353 (12)	n.s.	
in *Brp*^{RNAi} (Fig. S3d)		100.0 ± 15.41 (14)	7.639 ± 0.498 (15)	≤0.001***	(ANOVA test, followed by a Turkey's multiple comparison test)
in *Rbp*^{null} (Fig. S3d)			40.29 ± 3.292 (15)	≤0.001***	
in *Brp*^{RNAi}*;Rbp*^{null} (Fig. S3d)			4.135 ± 0.843 (13)	≤0.001***	
AZ density (Fig. S1d)	BRP spots/µm^2				
in *Syd-1*^{null} (Fig. S1d)		1.352 ± 0.058 (13)	1.057 ± 0.124 (11)	n.s.	(ANOVA test, followed by a Turkey's multiple comparison test)
in *Liprin-α*^{null} (Fig. S1d)			0.878 ± 0.132 (12)	≤0.01**	
mean Unc13A intensity (Fig. 3c, g; S1e; S3e)	measured over the whole NMJ (% of Wild type)				
in *Syd-1*^{null} (Fig. S1e)		100.0 ± 8.084 (13)	99.04 ± 11.50 (11)	n.s.	(ANOVA test, followed by a Turkey's multiple comparison test)
in *Liprin-α*^{null} (Fig. 3c, S1e)			79.36 ± 7.923 (12)	n.s.	
in *Brp*^{RNAi} (Fig. S3e)		100.0 ± 15.060 (14)	15.24 ± 1.916 (15)	≤0.001***	(ANOVA test, followed by a Turkey's multiple comparison test)
in *Rbp*^{null} (Fig. S3e)			23.88 ± 2.478 (15)	≤0.001***	
in *Brp*^{RNAi}*;Rbp*^{null} (Fig. 3g, Fig. S3e)			10.88 ± 1.117 (13)	≤0.001***	
Unc13A density (Fig. S1f; S3f)	Unc13A spots/µm²				
in *Syd-1*^{null} (Fig. S1f)		1.679 ± 0.088 (13)	1.322 ± 0.098 (11)	≤0.05*	(ANOVA test, followed by a Turkey's multiple comparison test)
in *Liprin-α*^{null} (Fig. S1f)			1.361 ± 0.110 (12)	n.s.	

in *Brp*^{RNAi} (Fig. S3f)	1.781 ± 0.106 (14)	0.442 ± 0.065 (15)	≤0.001***	(ANOVA test, followed by a Turkey's multiple comparison test)
in *Rbp*^{null} (Fig. S3f)		0.851 ± 0.094 (15)	≤0.001***	
in *Brp*^{RNAi};*Rbp*^{null} (Fig. S3f)		0.271 ± 0.052 (13)	≤0.001***	
mean Unc13B intensity (Fig. 3d, h; S1i; S3j)	measured over the whole NMJ (% of Wild type)			
in *Syd-1*^{null} (Fig. S1i)	100.0 ± 14.770 (11)	75.58 ± 7.521 (13)	n.s.	(ANOVA test, followed by a Turkey's multiple comparison test)
in *Liprin-α*^{null} (Fig. 3d, Fig. S1i)		29.52 ± 5.936 (15)	≤0.001***	
in *Brp*^{RNAi} (Fig. S3j)	100.0 ± 10.07 (12)	111.20 ± 11.60 (11)	n.s.	(ANOVA test, followed by a Turkey's multiple comparison test)
in *Rbp*^{null} (Fig. S3j)		109.20 ± 14.80 (13)	n.s.	
in *Brp*^{RNAi};*Rbp*^{null} (Fig. 3h, S3j)		140.7 ± 25.88 (10)	n.s.	
Unc13B density (Fig. S1j; S3k)	Unc13B spots/µm²			
in *Syd-1*^{null} (Fig. S1j)	1.592 ± 0.072 (11)	1.145 ± 0.069 (13)	≤0.01**	(ANOVA test, followed by a Turkey's multiple comparison test)
in *Liprin-α*^{null} (Fig. S1j)		0.382 ± 0.115 (15)	≤0.001***	
in *Brp*^{RNAi} (Fig. S3k)	0.910 ± 0.102 (12)	1.053 ± 0.119 (11)	n.s.	(ANOVA test, followed by a Turkey's multiple comparison test)
in *Rbp*^{null} (Fig. S3k)		0.886 ± 0.112 (13)	n.s.	
in *Brp*^{RNAi};*Rbp*^{null} (Fig. S3k)		1.060 ± 0.168 (10)	n.s.	
BRP ring diameter (Fig. S6b,d)	measured with STED microscopy (nm)			
in *Unc13A*^{null} (Fig. S6b)	191.0 ± 3.721 (9)	244.9 ± 3.045 (12)	≤0.001***	(Mann-Whitney U-test)
in *Unc13B*^{null} (Fig. S6d)	183.4.0 ± 1.421 (8)	182.3 ± 4.262 (8)	n.s.	(Mann-Whitney U-test)
mean Cac spot size (Fig. S6f)	% of control			
in *Unc13A*^{null}	100.0 ± 4.70 (19)	159.5 ± 6.65 (15)	≤0.001***	(Mann-Whitney U-test)
in *Unc13B*^{Null}		88.84 ± 3.819 (21)	n.s.	(Mann-Whitney U-test)
mean Cac intensity (Fig. S6g)	% of control			
in *Unc13A*^{null}	100.0 ± 8.543 (19)	113.1 ± 9.082 (15)	n.s.	(Mann-Whitney U-test)
in *Unc13B*^{null}		89.17 ± 8.146 (21)	n.s.	(Mann-Whitney U-test)

TEVC recordings (Fig. 4, 7; Fig. S4, S5)		**mean ± SEM**		
Parameter (Figure)	**Description**	**control (n)**	**mutant (n)**	**P**	**(test)**
eEJC amplitude [nA] in *Unc13A*^{null} (Fig. 4j; 7a, b)	measured (n) (simulated with mathematical modeling)				
$[Ca^{2+}]_{ex}$ = 0.75 mM		-26.10 ± 4.89 (12) (-18.34)	-1.82 ± 0.17 (12) (-1.589)	≤0.001***	(t- test)
$[Ca^{2+}]_{ex}$ = 1.5 mM		-77.46 ± 6.95 (12) (-63.58)	-4.88 ± 0.77 (12) (-6.471)	≤0.001***	(t- test)
$[Ca^{2+}]_{ex}$ =3 mM		-143.90 ± 8.07 (12) (-130.8)	-13.07 ± 1.13 (12) (-17.35)	≤0.001***	(t- test)
$[Ca^{2+}]_{ex}$ =6 mM		-193.96 ± 10.04 (12) (-187.6)	-30.86 ± 2.12 (12) (-30.20)	≤0.001***	(t- test)
$[Ca^{2+}]_{ex}$ =10 mM		-220.72 ± 13.94 (12) (-215.3)	-41.78 ± 3.09 (12) (-37.99)	≤0.001***	(t- test)
eEJC amplitude [nA] in *Unc13B*^{null} (Fig. 4c)					
$[Ca^{2+}]_{ex}$ = 0.75 mM		-30.64 ± 3.643 (12)	-20.17 ± 3.176 (12)	≤0.05*	(t- test)
$[Ca^{2+}]_{ex}$ =1.5 mM		-77.33 ± 6.383 (12)	-57.93 ± 5.026 (12)	≤0.05*	(t- test)
$[Ca^{2+}]_{ex}$ =3 mM		-138.3 ± 8.208 (12)	-117.3 ± 7.375 (12)	n.s.	(t- test)
$[Ca^{2+}]_{ex}$ =6 mM		-189.4 ± 11.54 (12)	-164.8 ± 8.270 (12)	n.s.	(t- test)
$[Ca^{2+}]_{ex}$ =10 mM		-224.1 ± 13.14 (12)	-190.9 ± 8.751 (12)	≤0.05*	(t- test)
time to peak [ms] in *Unc13A*^{null} (Fig. S4c)					
$[Ca^{2+}]_{ex}$ = 0.75 mM		3.892 ± 0.309 (12)	4.900 ± 0.760 (12)	n.s.	(t- test)
$[Ca^{2+}]_{ex}$ = 1.5 mM		3.117 ± 0.142 (12)	4.208 ± 0.394 (12)	≤0.05*	(t- test)
$[Ca^{2+}]_{ex}$ =3 mM		2.350 ± 0.120 (12)	3.017 ± 0.263 (12)	≤0.05*	(t- test)
$[Ca^{2+}]_{ex}$ =6 mM		1.925 ± 0.0913 (12)	2.600 ± 0.140 (12)	≤0.001***	(t- test)
$[Ca^{2+}]_{ex}$ =10 mM		1.883 ± 0.0694 (12)	2.275 ± 0.143 (12)	≤0.05*	(t- test)
time to peak [ms] in *Unc13B*^{null} (Fig. S4a)					
$[Ca^{2+}]_{ex}$ = 0.75 mM		4.225 ± 0.240 (12)	4.275 ± 0.332 (12)	n.s.	(t- test)
$[Ca^{2+}]_{ex}$ =1.5 mM		3.425 ± 0.0888 (12)	3.908 ± 0.297 (12)	n.s.	(t- test)
$[Ca^{2+}]_{ex}$ =3 mM		2.542 ± 0.0528 (12)	2.592 ± 0.119 (12)	n.s.	(t- test)

$[Ca^{2+}]_{ex}$ =6 mM		2.175 ± 0.0664 (12)	2.108 ± 0.114 (12)	n.s.	(t- test)
$[Ca^{2+}]_{ex}$ =10 mM		2.042 ± 0.106 (12)	1.950 ± 0.116 (12)	n.s.	(t- test)
mEJC analysis in *Unc13A*^{null} (Fig. 4m, n; S4g,h)					
Amplitude (nA)		-0.614 ± 0.02 (12)	-0.751 ± 0.02 (11)	≤0.001***	(t- test)
Frequency (Hz)		1.06 ± 0.12 (12)	1.41 ± 0.11 (11)	≤0.05*	(t- test)
Rise time (ms)		1.690 ± 0.129 (12)	1.451 ± 0.119 (11)	n.s.	(t- test)
Decay (ms)		6.299 ± 0.228 (12)	6.805 ± 0.376 (11)	n.s.	(t- test)
mEJC analysis [nA] in *Unc13B*^{null} (Fig. 4f, g; S4e,f)					
Amplitude (nA)		-0.859 ± 0.03 (14)	-0.837 ± 0.03 (7)	n.s.	(t- test)
Frequency (Hz)		2.08 ± 0.15 (14)	1.70 ± 0.23 (7)	n.s.	(t- test)
Rise time (ms)		1.127 ± 0.034 (14)	1.174 ± 0.078 (7)	n.s.	(Mann-Whitney U-test)
Decay (ms)		7.075 ± 0.398 (14)	8.931 ± 0.683 (7)	≤0.05*	(Mann-Whitney U-test)
eEJC analysis in *Unc13A*^{null} (Fig. 4k; S4d)					
Rise time (ms)		0.966 ± 0.052 (12)	2.0 ± 0.383 (9)	≤0.01**	(Mann-Whitney U-test)
Decay (ms)		5.627 ± 0.196 (12)	6.058 ± 0.425 (9)	n.s.	(Mann-Whitney U-test)
eEJC analysis [nA] in *Unc13B*^{null} (Fig. 4d; S4b)					
Rise time (ms)		1.125 ± 0.044 (12)	1.158 ± 0.101 (11)	n.s.	(t- test)
Decay (ms)		6.074 ± 0.181 (12)	6.706 ± 0.511 (11)	n.s.	(t- test)
paired pulse ratio in *Unc13A*^{null} (Fig. 7e)	measured (n) (simulated with mathematical modeling)				
$[Ca^{2+}]_{ex}$ = 0.75 mM		1.683 ± 0.308 (12) (1.273)	--	--	--
$[Ca^{2+}]_{ex}$ = 1.5 mM		0.904 ± 0.065 (12) (0.973)	3.796 ± 0.748 (10) (3.297)	≤0.001***	(t- test)
$[Ca^{2+}]_{ex}$ =3 mM		0.633 ± 0.021 (12) (0.635)	1.846 ± 0.264 (10) (2.128)	≤0.001***	(t- test)
$[Ca^{2+}]_{ex}$ =6 mM		0.631 ± 0.023 (12) (0.402)	1.309 ± 0.116 (10) (1.324)	≤0.001***	(t- test)
$[Ca^{2+}]_{ex}$ =10 mM		0.674 ± 0.035 (12) (0.304)	1.192 ± 0.111 (10) (0.986)	≤0.001***	(t- test)
paired pulse ratio in *Unc13B*^{null} (Fig. S5h)					
$[Ca^{2+}]_{ex}$ = 0.75 mM		1.255 ± 0.201 (12)	1.787 ± 0.245 (12)	n.s.	(t- test)

$[Ca^{2+}]_{ex}$ =1.5 mM	0.741 ± 0.079 (12)	0.974 ± 0.143 (12)	n.s.	(t- test)
$[Ca^{2+}]_{ex}$ =3 mM	0.637 ± 0.034 (12)	0.596 ± 0.044 (12)	n.s.	(t- test)
$[Ca^{2+}]_{ex}$ =6 mM	0.503 ± 0.117 (12)	0.614 ± 0.0316 (12)	n.s.	(t- test)
$[Ca^{2+}]_{ex}$ =10 mM	0.680 ± 0.043 (12)	0.619 ± 0.029 (12)	n.s.	(t- test)
I/I_{Max} in *Unc13A*^{null} (Fig. 7c; S5a)	measured (n) (simulated with mathematical modeling)			
$[Ca^{2+}]_{ex}$ = 0.75 mM	0.110 ± 0.020 (12) (0.079)	0.033 ± 0.003 (10) (0.036)	≤0.01**	(t- test)
$[Ca^{2+}]_{ex}$ = 1.5 mM	0.327 ± 0.029 (12) (0.274)	0.089 ± 0.014 (10) (0.146)	≤0.001***	(t- test)
$[Ca^{2+}]_{ex}$ =3 mM	0.608 ± 0.034 (12) (0.563)	0.240 ± 0.020 (10) (0.390)	≤0.001***	(t- test)
$[Ca^{2+}]_{ex}$ =6 mM	0.820 ± 0.042 (12) (0.808)	0.560 ± 0.039 (10) (0.679)	≤0.05*	(t- test)
$[Ca^{2+}]_{ex}$ =10 mM	0.934 ± 0.058 (12) (0.927)	0.768 ± 0.056 (10) (0.854)	≤0.01**	(t- test)
I/I_{Max} in *Unc13B*^{null} (Fig. S5d)				
$[Ca^{2+}]_{ex}$ = 0.75 mM	0.096 ± 0.015 (12)	0.120 ± 0.014 (12)	n.s.	(t- test)
$[Ca^{2+}]_{ex}$ =1.5 mM	0.277 ± 0.024 (12)	0.303 ± 0.025 (12)	n.s.	(t- test)
$[Ca^{2+}]_{ex}$ =3 mM	0.562 ± 0 035 (12)	0.542 ± 0.032 (12)	n.s.	(t- test)
$[Ca^{2+}]_{ex}$ =6 mM	0.790 ± 0.039 (12)	0.743 ± 0.045 (12)	n.s.	(t- test)
$[Ca^{2+}]_{ex}$ =10 mM	0.915 ± 0.041 (12)	0.879 ± 0.053 (12)	n.s.	(t- test)
K_D and slope in *Unc13A*^{null} (Fig. S5b,c)	values of fitted Hill coefficients			
K_D (mM)	2.048 ± 0.160 (12)	8.063 ± 1.537 (10)	≤0.001***	(Mann-Whitney U-test)
slope	1.922 ± 0.2003 (12)	2.079 ± 0.232 (10)	n.s.	(Mann-Whitney U-test)
K_D and slope in *Unc13B*^{null} (Fig. S5e, f)	values of fitted Hill coefficients			
K_D (mM)	2.966 ± 0.273 (12)	2.987 ± 0.265 (12)	n.s.	(Mann-Whitney U-test)
slope	1.501 ± 0.096 (12)	1.751 ± 0.140 (12)	n.s.	(Mann-Whitney U-test)
normalized residual amplitude in *Unc13A*^{null} (Fig. 7g; S5i)	**with 200µM EGTA-AM/DMSO** in the extracellular solution; measured (n) (simulated with mathematical modeling)			
after 3 min	0.784 ± 0.031 (10) (0.821)	0.530 ± 0.048 (10) (0.512)	≤0.001***	(t- test)
after 6 min	0.671 ± 0.040 (10) (0.741)	0.434 ± 0.073 (10) (0.382)	≤0.05*	(t- test)

after 9 min		0.592 ± 0.055 (10) (0.699)	0.379 ± 0.066 (10) (0.303)	≤0.05*	(t- test)
after 12 min		0.569 ± 0.058 (10) (0.677)	0.354 ± 0.038 (10) (0.300)	≤0.01**	(t- test)
normalized residual eEJC amplitude in *Unc13A*^{null} (Fig. S5i)	**with DMSO** in the extracellular solution (control)				
after 3 min		0.960 ± 0.029 (10)	0.8660 ± 0.077 (10)	n.s.	(t- test)
after 6 min		0.949 ± 0.015 (10)	0.8216 ± 0.081 (10)	n.s.	(t- test)
after 9 min		0.934 ± 0.012 (10)	0.8145 ± 0.085 (10)	n.s.	(t- test)
after 12 min		0.921 ± 0.014 (10)	0.8554 ± 0.111 (10)	n.s.	(t- test)
Decay and plateau in *Unc13A*^{null} (Fig. S5j, k)	values of single exponential fit to amplitude (normalized) decay **upon 200 µm EGTA-AM/DMSO application**				
tau (s)		264.5 ± 32.94 (10)	122.8 ± 16.73 (10)	≤0.01**	(t- test)
plateau		0.530 ± 0.057 (10)	0.354 ± 0.033 (10)	≤0.05*	(t- test)
total residual eEJC amplitude in *Unc13A*^{null} (Fig. S5m, n, o)	upon incubation with **100µM Bapta-AM/DSMO**				
DMSO (Ctrl): amplitude (nA)	after 30 min	-116.9 ± 8.033 (15)	9.707 ± 2.224 (14)	≤0.001***	(t- test)
Bapta-AM: amplitude (nA)	after 30 min	-9.481 ± 1.921 (14)	-0.591±0.096 (14)	≤0.001***	(t- test)
Bapta sensitivity		0.081 ± 0.016 (14)	0.060 ± 0.009 (14)	n.s.	(t- test)

Supplementary Table 2: Model values (dual pathway model)				
Parameter name	**Value**	**Unit**	**Description**	**Source**
$dist_1$	76.8	nm	Pathway 1: Distance from Ca^{2+} source and RRP size	best fit
R0A	670	vesicles		
$dist_2$	145	nm	Pathway 2: Distance from Ca^{2+} source and RRP size	
R0B	196	vesicles		
Q_{max} (Wild type)	2.57	fC	max Ca^{2+} channel charge in Wild type AZs (see equation (2))	
Q_{max} (*Unc13A*^{null})	4.41	fC	max Ca^{2+} channel charge in *Unc13A*^{null} AZs (see equation (2))	
K_M	1.74	mM	Michaelis-Menten constant to calculate dependence of synaptic Ca^{2+} current on extracellular $[Ca^{2+}]$ (see equation (2))	
$[EGTA]_{max}$	3925	µM	asymptotic value and time constant of exponential $[EGTA]_{int}$ increase (see equation (1))	
τ_{EGTA}	5.12	min		
Further Parameters				
Parameter name	**Value**	**Unit**	**Description**	**Source**
L^+	$3.5 \cdot 10^{-4}$	s^{-1}	basal fusion rate constant of [R]	Kochubey&Schneggenburger, 2011. Neuron. 69:736-748.
k_3	$1.4 \cdot 10^8$	$M^{-1} \cdot s^{-1}$	rate constants of Ca^{2+} binding/release	
k_{-3}	4000	s^{-1}		Wolfel et al., 2007. J. Neurosci. 27:3198-3210.
k_4	6000	s^{-1}	fusion rate constant of $[RCa_5]$	Lou et al., 2005. Nature. 435:497-501.
b	0.5	-	cooperativity factor	Wolfel et al., 2007. J. Neurosci. 27:3198-3210.